Mon. Not. R. Astron. Soc. **266,** L27–L39 (1994)

Optical observations of supernova 1993J from La Palma – I. Days 2 to 125

James R. Lewis,[1] N. A. Walton,[2] W. P. S. Meikle,[1]★ R. Martin,[1] Robert J. Cumming,[1] R. M. Catchpole,[1] M. Arévalo,[3] R. W. Argyle,[1] C. R. Benn,[2] P. S. Bunclark,[1,2] H. O. Castañeda,[2,4] M. Centurión,[4] R. E. S. Clegg,[1] A. Delgado,[3] V. S. Dhillon,[2] P. Goudfrooij,[5] E. H. Harlaftis,[2] B. J. M. Hassall,[1] L. Helmer,[6] P. W. Hill,[7] D. H. P. Jones,[1,2] D. L. King,[1] C. Lázaro,[4] J. R. Lucey,[8] E. L. Martín,[4] L. Miller,[9] L. V. Morrison,[1] A. J. Penny,[10] E. Pérez,[4] M. Read,[9] P. J. Rudd,[2] R. G. M. Rutten,[2] R. M. Sharples,[8] S. W. Unger[2] and J. Vilchez[4]

[1]*Royal Greenwich Observatory, Madingley Road, Cambridge CB3 0EZ*
[2]*Isaac Newton Group, Royal Greenwich Observatory, Apartado 321, 38780 Santa Cruz de La Palma, Canary Islands, Spain*
[3]*Instituto de Astrofísica de Andalucia, CSIC, Apdo 3004, 1808 Granada, Spain*
[4]*Instituto de Astrofísica de Canarias, La Laguna, 38200 Tenerife, Spain*
[5]*Astronomical Institute 'Anton Pannekoek', University of Amsterdam, Kruislaan 403, NL-1098 SJ Amsterdam, The Netherlands*
[6]*Copenhagen University Observatory, Brorfeldevej 23, Tølløse, DK4340, Denmark*
[7]*Department of Physics and Astronomy, University of St Andrews, North Haugh, St Andrews, Fife KY16 9SS*
[8]*Department of Physics, University of Durham, South Road, Durham DH1 3LE*
[9]*Royal Observatory, Blackford Hill, Edinburgh EH9 3HJ*
[10]*Rutherford Appleton Laboratory, Chilton, Didcot, Oxon OX11 0QX*

Accepted 1993 November 5. Received 1993 November 3; in original form 1993 October 7

ABSTRACT

We present astrometric, photometric and spectroscopic observations of supernova 1993J in M81, obtained with the Isaac Newton Group telescopes and the Carlsberg Automatic Meridian Circle. The spectral data set includes the first spectrum ever taken of SN1993J. The early spectra also yield an estimate of the total visual extinction, A_V. This is combined with the photometric data to produce a bolometric light curve. Implications of the latter and of the spectral development are also discussed. The spectral evolution includes an infrared excess, which appeared after day 50 and may be indicative of an IR echo. The unchanging nature of blueshifted oxygen lines in the spectra argues for asymmetry in the distribution of the line-emitting region.

Key words: dust, extinction – supernovae: individual: 1993J – galaxies: individual: M81.

1 INTRODUCTION

Supernova (SN) 1993J was visually discovered in a spiral arm of M81 (NGC 3031) at 21.45 UT on 1993 March 28 by F. García-Diaz (García 1993; Kato 1993). It was confirmed with an unfiltered CCD observation half an hour later (Rodriguez 1993; Kato 1993). From spectra obtained on March 30.25 UT (Garnavich & Ann 1993) and on March 30.3 UT (Filippenko et al. 1993b), the event was identified as being probably of Type II. Later spectra confirmed this. Its V magnitude peaked at +10.7 on March 30, making this event the brightest of its type this century, apart from SN1987A, and *the* brightest accessible to the major northern observatories.

The earliest measurement of supernova 1993J was by Neely (1993a), who obtained a CCD detection 14.5 h before García-Diaz's discovery. Neely (1993b) converted his preliminary unfiltered CCD magnitude, obtaining a Johnson V magnitude of +13.45. Only 9 h before Neely's measurement, Merlin (1993) failed to detect the event at a limiting magnitude (Ektachrome 400) of +16.0. The supernova was therefore clearly caught on the rise, and it rose rapidly. The most recent measurement of the pre-explosion stellar image was on 1993 March 23 by Prugniel (1993), who

★ Present address: Blackett Laboratory, Imperial College of Science, Technology and Medicine, Prince Consort Road, London SW7 2BZ.

obtained an R_C magnitude of +19.9. If we assume that the progenitor indeed had a magnitude of about this value, and if we also assume that the supernova was no more than 0.3 mag brighter than Merlin's limit at the epoch of his observation, then the range of linear extrapolations (in a magnitude versus time plot) possible down to +19.9, consistent with the Merlin limit minus 0.3 and the Neely point, indicates an explosion date between March 26.9 and 28.3. We therefore adopt 1993 March 27.5 (JD 244 9074.0) as the explosion date in this paper (hereafter referred to as t_0). The epoch of core collapse was probably about 0.1 d earlier than this (Woosley et al. 1993; Shigeyama et al. 1993).

Of particular importance is that the distance of SN1993J is accurately known from Cepheid variable measurements in M81 (e.g. Freedman et al. 1993). This precision means that absolute measurements of the supernova energetics are considerably more precise than is usually possible for supernovae. Moreover, its close proximity means that high-quality optical spectroscopy should continue to be feasible well into the nebular phase, when we can obtain a direct view of the supernova constituents.

Upon the announcement of the supernova discovery, it was immediately recognized that the Isaac Newton Group (ING) of telescopes and the Carlsberg Automatic Meridian Circle (CAMC) on La Palma could provide excellent optical coverage of this important event. A programme was quickly organized to acquire astrometric, photometric and spectroscopic observations. This involved contributions from the ING and from the CAMC. The ING comprises the 1-m Jacobus Kapteyn Telescope (JKT), the 2.5-m Isaac Newton Telescope (INT) and the 4.2-m William Herschel Telescope (WHT). The first spectrum was obtained at 21.00 UT on March 29, less than a day after the discovery observation, and probably within a few hours of the first maximum at *V*. This was the earliest spectrum obtained of SN1993J at any wavelength, anywhere.

In this paper we present, and briefly discuss, the results of the first 125 d of the monitoring programme on La Palma. This includes astrometric measurements by the CAMC, broad-band *UBVRI* photometry, mainly by the JKT, and spectroscopic observations taken with the INT and WHT. High-dispersion echelle spectroscopy was also carried out on the WHT, but this will be presented elsewhere (e.g. Vladilo et al. 1993). The raw data were all reduced following the same procedure, thus providing an internally consistent set of results.

2 ASTROMETRY

It is important to determine as accurately as possible the position of the supernova. This is vital for late-time spectroscopic studies when the supernova can no longer be viewed on the TV finder. In addition, precise knowledge of the supernova position assists in the identification of the progenitor on pre-explosion images. Astrometry was carried out with the CAMC. This is equipped with a scanning-slit micrometer and photomultiplier, as well as a CCD system for registering the pointing angle of the telescope. A detailed description of the system can be found in Helmer, Fabricius & Morrison (1991). Using this system, the accurate positions of stars and other objects are measured relative to a version of the FK5 reference system in which many of the zonal errors have been smoothed out (see Morrison et al. 1990). The systematic errors of the CAMC positions are thought to be less than 0.05 arcsec. The quoted errors (below) of 0.10 arcsec for the position of SN1993J include a contribution for this systematic error.

The CAMC made 10 measurements of the position of SN1993J, obtained during the period April 2–25. The observations were made in the Johnson *V* band. After April 25, SN1993J transited during daylight and was hence no longer observable. The mean optical position of SN1993J obtained from the CAMC measurements is

RA	$09^h55^m24^s.785$,
Dec.	$+69°01'13''.69$,
Equinox	J2000.0,
Epoch	1993.27 on the FK5 system,

with a conservatively estimated error of 0.10 arcsec in RA and Dec.

This position supersedes that given by Morrison, Argyle & Helmer (1993). Marcaide et al. (1993) obtained a J2000 VLBI radio position of $\alpha = 09^h55^m24^s.7740 \pm 0^s.0006$, $\delta = +69°01'13''.700 \pm 0''.003$. This position agrees with the CAMC optical position, to within the errors, providing a useful consistency check between the optical and radio reference frames.

3 THE PROGENITOR

Two CCD frames at *R* (KPNO filter) of the M81 region were taken on 1991 October 10 by E. Telles, and they include the supernova progenitor location. The sum of the two images is shown in Fig. 1(a) (opposite p. L28). These observations were made using the CCD camera at the INT prime focus with a blue-coated Ford CCD. The chip has a 2048×2048 format of 15-μm pixels, which gives a scale of 0.4 arcsec per pixel. The seeing was 3 arcsec. The total exposure time for the two frames was 450 s. (A contrast-enhanced version of this image is shown in Fig. 2, opposite p. L28.) A CCD frame at *V* (also KPNO filter) of the M81 region was also taken by E. Telles, on 1992 March 23. These observations were also made using the INT's CCD camera, but this time with an EEV 530 chip (see next section) as the detector. The seeing was 2 arcsec and the exposure time was 300 s.

Inspection of the pre-explosion *V* and *R* CCD images revealed an unresolved image lying coincident with the supernova position, within the errors. This can be seen in the *R*-band image (Fig. 1). We have derived photometry of this point image using the photometric local standard star C (see next section). The magnitudes of the stellar image identified at the position of SN1993J are $V = 20.7 \pm 0.2$ and $R = 19.8 \pm 0.2$. These are in good agreement with the photometry reported by Humphreys et al. (1993), who determined magnitudes of $V = 20.8 \pm 0.1$ and $R = 19.9 \pm 0.2$ obtained from automated plate scanner measurements of 1982 prime-focus plates of the field of SN1993J. There is no obvious evidence of blending in our images.

4 PHOTOMETRY

4.1 Observations

Most of the photometry was obtained with the CCD camera at the *f*/15 Cassegrain focus of the JKT (Argyle et al. 1988).

(a)

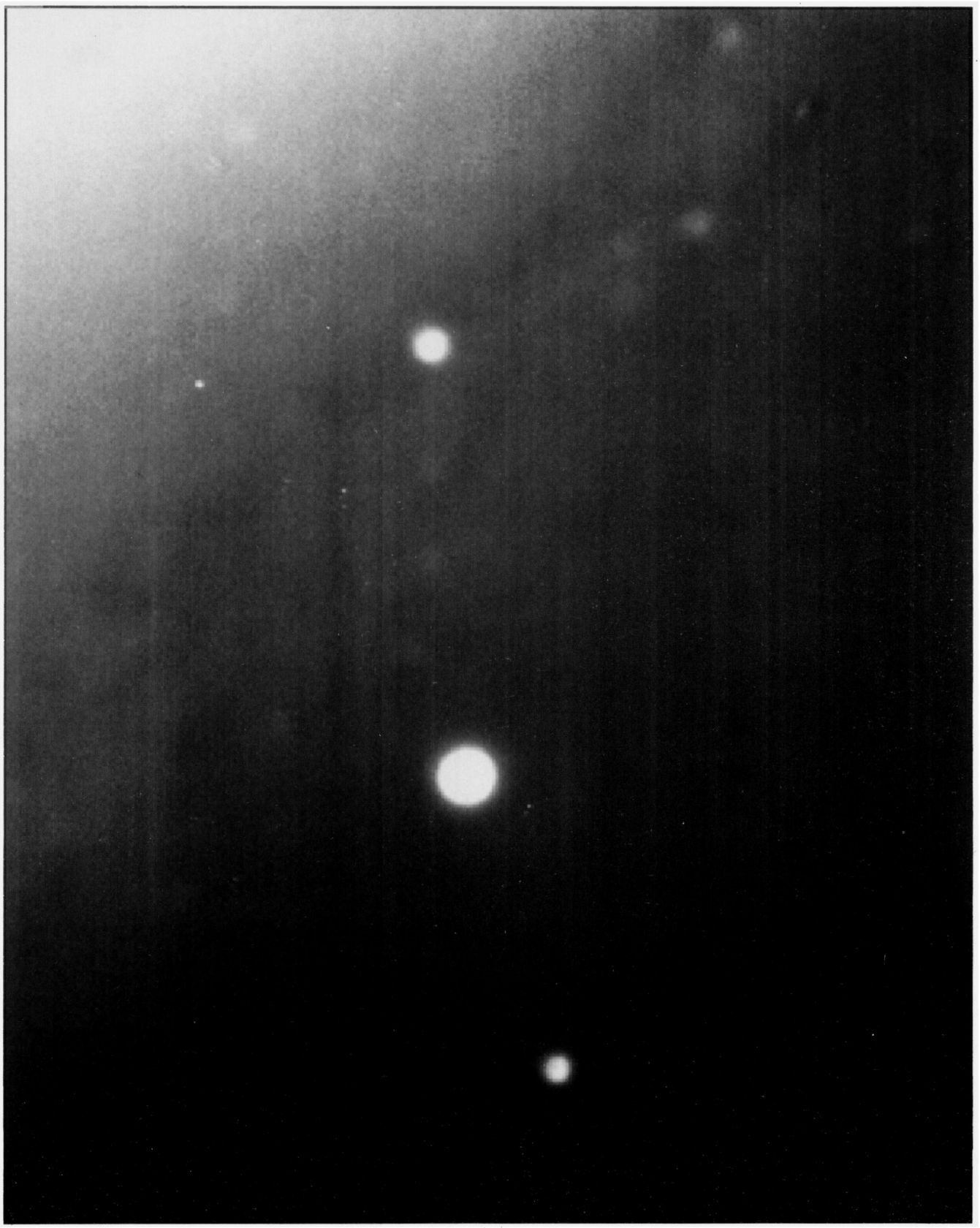

Figure 1. (a) A section of a sum of two *R*-band CCD frames of M81 taken on the INT on 1991 October 10 by E. Telles. This section includes the supernova progenitor region. The likely progenitor is just discernible mid-way between the two brightest stars. The photometric local standard star C is the brightest on this image. (b) The same region but now after the supernova explosion. This latter *R*-band image was obtained on 1993 April 7, approximately 8 d after SN1993J reached its maximum optical luminosity. North is up and east is to the left.

(b)

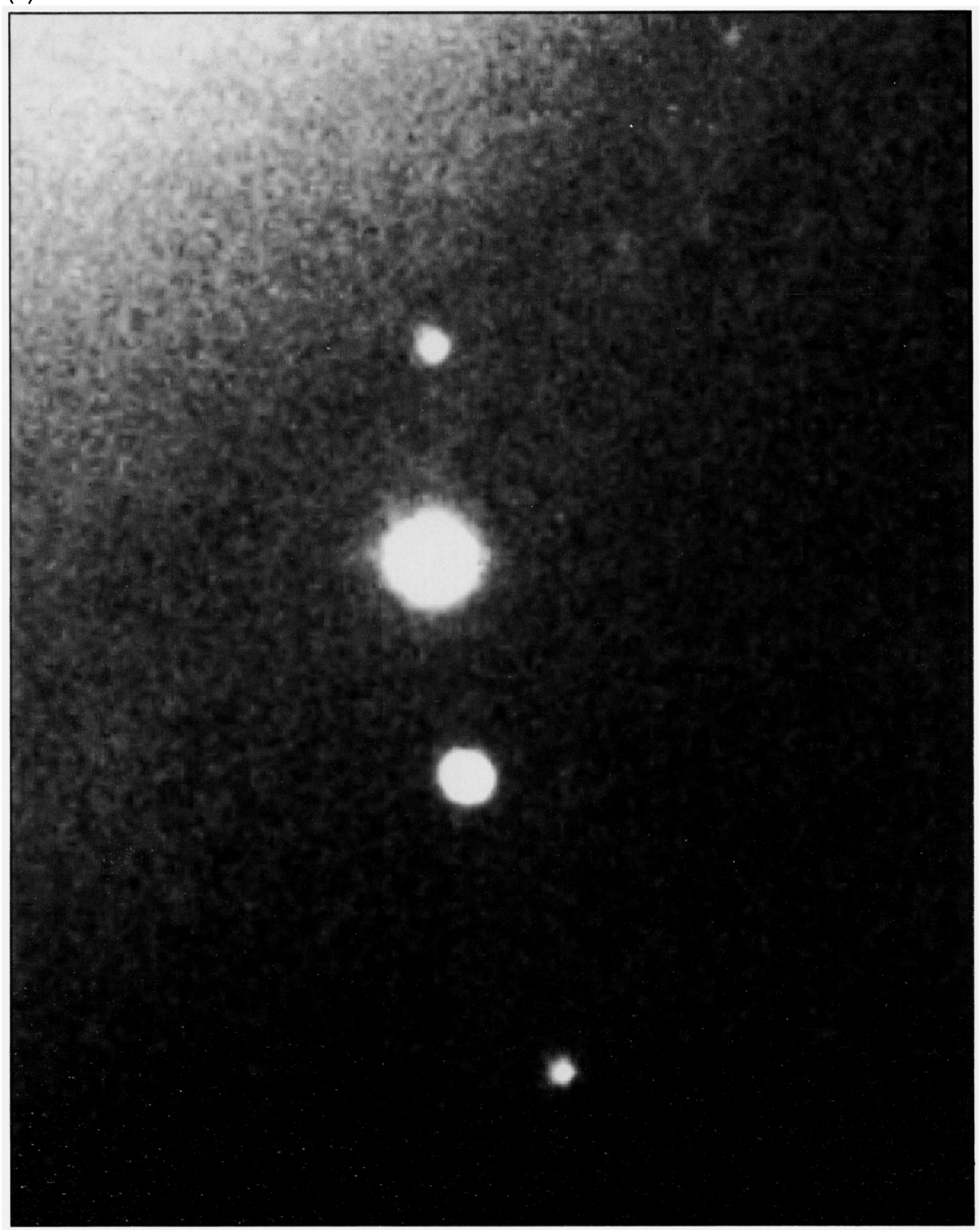

Figure 1 – *continued*

Opposite p. L28, MNRAS, **266**

Figure 2. A contrast-enhanced view of the progenitor image seen in Fig. 1. The progenitor is marked with an arrow. Again, north is up and east is to the left.

On every night that SN1993J was observed with the JKT, *BVI* photometry was obtained, with somewhat less frequent measurements in *U* and *R* due to the filter requirements of the scheduled observing programmes. In almost all instances the Harris filters were used, which have *R* and *I* bands similar to those in the Cousins system (Benn & Nicholson 1988). The detector was an EEV 0530 chip with a format of 1242×1152 pixels, giving a coverage of 6.5×6 arcmin^2. This field size made possible *simultaneous* measurement of the supernova and a number of nearby stars lying within 2 arcmin, which were used as local flux standards. A Coradograph was used to obtain the positions of the local standards from the POSS O plate, relative to eight astrometric standards. These positions are listed in Table 1. The error is about 1 arcsec in both coordinates. Early in the programme a number of photometric standards, selected from the lists of Landolt (1983, 1992), were also observed each night.

Additional photometric measurements were made using the CCD camera at the $f/3.3$ prime focus of the INT. An EEV 530 CCD was used as detector, the chip size being 1242×1152 0.6-arcsec pixels, giving a field of $\approx 11.5 \times 10.7$ arcmin^2.

4.2 Reduction and results

The frames containing the supernova and flux standard images were debiased and flat-fielded in the usual manner. Instrumental magnitudes were then obtained by defining an aperture around the image and summing the counts within this region. The size of the aperture was varied according to the seeing on the particular night, and was typically twice the FWHM of a stellar image. The local sky was estimated from an annulus outside the aperture.

On nights when such information was available, the supernova and local standard magnitudes were determined directly from the Landolt standards. At least 10 photometric measurements of each local standard were obtained, yielding the mean magnitudes given in Table 1. None of the local standard stars exhibited variability exceeding ~0.03 mag in *V* over the 2-week period when this 'absolute' photometry was being done, nor did the local standards show any detectable relative variability over the period of this study. On nights when no Landolt stars were observed, the supernova magnitudes were measured relative to these local standard magnitudes. Comparisons of the supernova magnitudes derived by both methods on nights where Landolt standard observations were available show a mean deviation of only 0.03 mag. The results of the photometry are listed in Table 2. The numbers in parentheses represent the internal errors in thousandths of a magnitude.

4.3 Light curves

Fig. 3 shows the photometric data from Table 2 plotted as light curves. Even by the epoch of our earliest photometry (day 3.4) the supernova was fading in all five bands. Our photometry, together with earlier measurements by others made between days 0.8 and 2.7 (Neely 1993a; Rodriguez 1993; Ulfheden & Hamberg 1993; Solberg 1993; Richmond 1993a), suggests that *V* maximum was within a few hours of 3.0 d after t_0. The decline after day 3.0 was steeper at shorter wavelengths, presumably due to the cooling of the expanding photosphere. The decline halted on day 8.5 (± 0.5 d) at *BVRI*, and about a day later at *U*. The supernova then brightened to a second maximum in *B* and *V* on day 20.5 (April 17.0), with *I* peaking about two days later.

The decline after day 20.5 exhibits two distinct phases. Up to about day 38, the *V* magnitude declined at 0.083 mag d^{-1}, with the shorter wavelength fluxes declining faster and the longer slower, indicating continuing cooling of the ejecta. After day 38, however, the decline slowed considerably. *V* faded at 0.018 mag d^{-1}, with the longer wavelength fluxes now declining *faster* and the shorter *slower*. Indeed, from about day 50 to day 125, the *U*-band flux remained almost constant.

5 SPECTROSCOPY

5.1 Observations

Low-resolution spectra were obtained every night between days 2.4 and 15.4, and less frequently thereafter. Most of the spectra were obtained with the INT, with additional spectra being obtained with the WHT. Spectral coverage and resolution varied depending on the different instrumental configurations of the scheduled observing programmes. Typically, the spectral range was 3500 to 9500 Å, and the resolution (2 pixel) 5 to 10 Å.

At the INT, the spectra were obtained with the Intermediate Dispersion Spectrograph (IDS) (Terlevich, Terlevich & Charles 1989). The detector was usually an EEV 530 CCD, with 1242×1152 pixels. For all but the lowest resolution spectra, full spectral coverage was achieved by observing at two grating settings and then merging the spectra. The WHT spectroscopy was carried out using the dual-beam intermediate-dispersion spectrograph ISIS (Clegg et al. 1992). On nights when the ISIS red arm was not available, spectra were obtained using the Faint Object Spectrograph (FOS2) (Allington-Smith et al. 1989).

For all spectroscopic observations, SN1993J was observed with the slit at the parallactic angle (to minimize possible differential light losses due to atmospheric

Table 1. Positions (J2000) and photometry of local standards. In parentheses are the mean internal errors in thousandths of a magnitude.

Name	α	δ	V	(B–V)	(U–B)	(V–R)	(R–I)	(V–I)
Star A	$9^h55^m45^s.0$	+69°01′44″.0	11.432(2)	0.530(5)	0.055(9)	0.342(5)	0.305(6)	0.647(7)
Star B	$9^h55^m41^s.1$	+69°00′30″.0	11.898(2)	0.490(4)	–0.069(7)	0.330(4)	0.305(5)	0.635(6)
Star C	$9^h55^m23^s.5$	+69°00′49″.0	14.490(19)	0.556(41)	–0.011(62)	0.394(35)	0.307(42)	0.701(51)

Table 2. *UBVRI* photometry of SN1993J. All photometry comes from the JKT, with the exception of those with an asterisk after the date (which are INT prime focus). In parentheses are the internal errors in thousandths of a magnitude.

Date (UT)	ΔD	V	(B–V)	(U–B)	(V–R)	(R–I)	(V–I)
Mar 30.89	3.39	10.704(4)	0.075(7)	-0.872(8)	0.106(4)	0.089(2)	0.195(4)
Mar 31.06	3.56	10.764(4)	0.091(6)	-0.880(6)	0.125(4)	0.089(4)	0.214(6)
Mar 31.98	4.48	11.038(3)	0.176(6)	-0.683(6)	0.221(4)	0.159(4)	0.380(6)
Apr 01.90	5.40	11.296(4)	0.265(5)	-0.522(4)	0.242(5)	0.233(5)	0.475(7)
Apr 02.08	5.58	11.357(3)	0.308(5)	-0.560(4)	0.299(4)	0.207(5)	0.475(6)
Apr 02.99	6.49	11.604(2)	0.324(4)	-0.470(4)	0.302(4)	0.272(5)	0.574(6)
Apr 03.16	6.66	11.654(2)	0.333(4)	-0.414(5)	0.356(4)	0.271(5)	0.627(6)
Apr 03.90	7.40	11.786(2)	0.331(5)	-0.436(6)	0.361(5)	0.257(8)	0.618(9)
Apr 04.09	7.59	11.865(3)	0.361(6)	-0.446(8)	0.368(7)	0.291(9)	0.659(11)
Apr 04.95	8.45	11.899(2)	0.378(4)	-0.424(4)	0.399(4)	0.243(5)	0.642(6)
Apr 05.08	8.58	11.914(2)	0.370(4)	-0.407(5)	0.410(4)	0.238(5)	0.648(6)
Apr 05.91	9.41	11.835(2)	0.425(3)	-0.331(4)	0.388(4)	0.219(7)	0.607(8)
Apr 05.97	9.47	11.876(4)	0.377(5)	-0.312(5)	0.426(6)	0.225(8)	0.651(10)
Apr 06.10	9.60	11.839(2)	0.402(4)	-0.324(6)	0.393(4)	0.218(7)	0.621(8)
Apr 06.99	10.49	11.796(2)	0.418(4)	-0.258(5)	0.411(6)	0.187(13)	0.598(14)
Apr 08.02*	11.52	11.641(2)	0.424(4)	-0.189(7)	0.395(2)	0.177(2)	0.572(3)
Apr 08.10	11.60	11.639(2)	0.419(3)	-0.183(4)	0.390(4)	0.187(4)	0.533(6)
Apr 08.98	12.48	11.517(0)	0.409(2)	-0.131(4)	0.387(2)	0.158(5)	0.565(5)
Apr 10.07	13.57	11.394(4)	0.449(5)	-0.125(4)	0.380(5)	0.142(6)	0.481(8)
Apr 10.16	13.66	11.392(4)	0.431(5)	-0.106(5)	0.379(6)	0.133(6)	0.417(8)
Apr 10.89	14.39	11.290(1)	0.450(2)	-0.106(3)	0.436(2)	0.070(3)	0.506(4)
Apr 10.93	14.43	11.313(1)	0.411(2)	-0.089(3)	0.457(2)	0.095(4)	0.552(4)
Apr 11.01	14.51	11.285(1)	0.438(2)	-0.093(3)	0.430(2)	0.071(4)	0.501(4)
Apr 11.06	14.56	11.317(2)	0.411(3)	-0.104(3)	0.469(3)	0.073(4)	0.542(5)
Apr 11.93	15.43	11.177(1)	0.466(2)				0.487(3)
Apr 12.87	16.37	11.101(1)	0.427(2)				0.460(3)
Apr 13.00	16.50	11.090(2)	0.457(3)				0.467(5)
Apr 13.88	17.38	11.013(1)	0.476(2)				0.467(3)
Apr 14.04	17.54	11.002(1)	0.476(2)				0.462(3)
Apr 14.88	18.38	10.947(1)	0.481(2)				0.451(3)
Apr 14.98	18.48	10.942(1)	0.481(1)				0.469(3)
Apr 15.88	19.38	10.898(1)	0.501(2)				0.454(3)
Apr 16.05	19.55	10.904(0)	0.508(2)				0.468(3)
Apr 16.89	20.39	10.863(1)	0.527(2)				0.441(3)
Apr 17.00	20.50	10.856(1)	0.541(2)				0.462(3)
Apr 17.93	21.43	10.896(1)	0.516(2)				0.514(3)
Apr 21.96	25.46	10.997(1)	0.759(2)		0.432(2)	0.152(4)	0.584(4)
Apr 23.91	27.41	11.175(1)	0.900(2)		0.501(1)	0.180(2)	0.681(2)
Apr 24.89	28.39	11.245(0)	0.993(2)		0.418(0)	0.225(0)	0.643(1)
Apr 25.91*	29.41	11.328(1)	1.075(3)	0.517(4)	0.496(1)	0.237(1)	0.733(1)
Apr 25.91	29.41	11.357(2)	1.047(3)	0.542(5)	0.583(3)	0.163(3)	0.746(4)
Apr 27.91	31.41	11.521(1)	1.161(3)	0.649(6)	0.632(2)	0.164(3)	0.796(4)
Apr 28.87	32.37	11.615(1)	1.216(4)	0.635(7)	0.671(2)	0.165(4)	0.836(4)
Apr 29.90	33.40	11.675(2)	1.182(3)	0.773(7)	0.680(3)	0.193(4)	0.873(5)
Apr 30.88	34.38	11.736(2)	1.240(5)	0.741(9)	0.692(2)	0.191(3)	0.883(4)
May 05.89	39.30	12.004(2)	1.276(6)	0.794(19)	0.715(3)	0.257(3)	0.973(4)
May 14.90	48.40	12.262(2)	1.284(4)	0.904(12)	0.690(3)	0.290(4)	0.980(5)
May 15.90	49.40	12.311(1)	1.266(3)	0.790(8)	0.710(1)	0.292(2)	1.002(2)
May 16.88	50.38	12.329(1)	1.290(4)				1.017(2)
May 18.99	52.49	12.381(2)	1.255(6)		0.688(3)		
May 22.88	56.38	12.456(2)	1.234(5)	0.708(12)	0.721(3)	0.270(4)	0.991(5)
May 24.91	58.41	12.493(2)	1.245(7)	0.721(17)	0.672(3)	0.344(3)	1.016(4)
May 25.88	59.38	12.509(3)	1.216(6)	0.690(13)	0.662(4)	0.330(4)	0.992(6)
Jun 19.90	84.40	12.959(4)	0.961(10)	0.411(20)	0.563(6)	0.375(6)	0.938(8)
Jun 20.94	85.44	12.983(2)	0.942(4)	0.446(9)	0.589(3)	0.356(3)	0.945(4)
Jun 21.92	86.42	12.991(2)	0.944(4)	0.411(10)	0.580(3)	0.354(3)	0.936(4)
Jun 23.92	88.42	13.034(1)	0.927(4)	0.398(9)	0.590(1)		
Jul 15.94	110.44	13.445(3)	0.739(9)	0.297(14)	0.488(4)	0.400(5)	0.888(6)
Jul 30.93	125.43	13.759(10)	0.578(35)	0.380(65)	0.473(18)	0.388(17)	0.861(25)

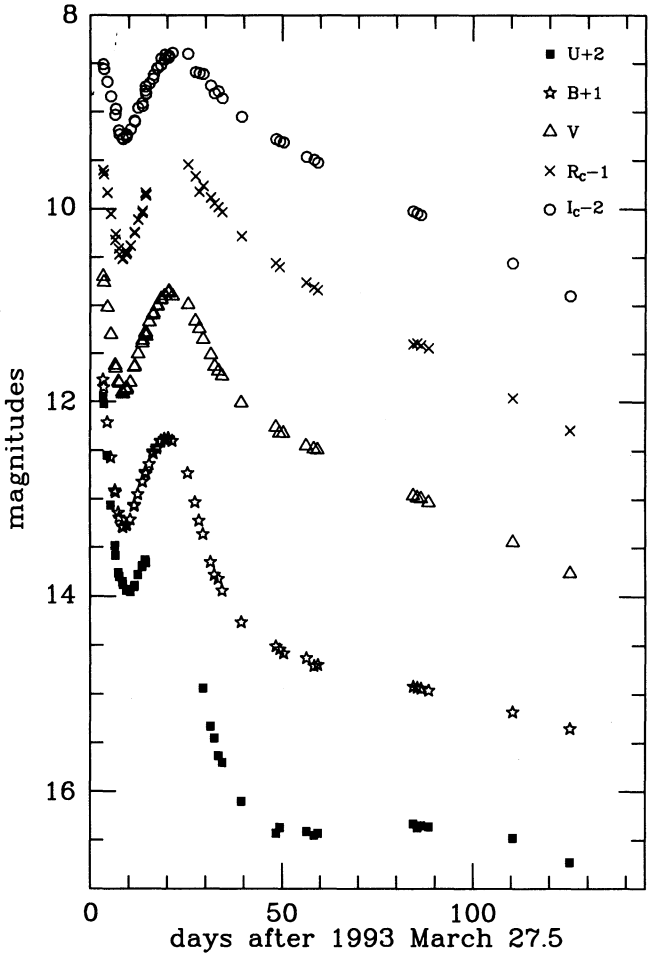

Figure 3. Light curves for SN1993J. The colours are represented by the following symbols: *U*, filled squares; *B*, stars; *V*, open triangles; R_C, crosses; I_C, open circles. The individual light curves have been shifted by amounts specified in the figure for the sake of clarity.

diffraction), with sufficient sky on both sides of the SN to ensure adequate sky subtraction. In all cases narrow-slit observations were obtained, the slit width being typically set to match 2 pixel at the detector (i.e. slit widths of 0.8 arcsec for the INT+IDS+500 camera, 1.5 arcsec for the INT+IDS+235 camera, and ≈1.0 arcsec for WHT+ISIS observations). Some wide-slit (>5 arcsec) observations were also obtained, and these were found to have line ratios and continuum slopes identical to those of the narrow-slit spectra. We conclude that contamination of the supernova spectra by extended emission was negligible.

On all nights a spectrophotometric flux standard was observed (with a few exceptions when the observing programme was interrupted by bad weather) – this was generally the star Feige 34 (Massey et al. 1988). When time permitted, a spectrum was also taken of the local spectrophotometric standard, star B. When conditions were photometric, the standards (and supernova) were observed through a wide slit (>5 arcsec).

5.2 Reduction and results

Table 3 shows the log of all low-resolution spectroscopic observations for days 2 to 115 (1993 March 29–July 20): column 1, date of the observation; column 2, number of days since 1993 March 27.5 (t_0); column 3, telescope and instrument [for INT+IDS the camera employed is also shown (e.g. INT/IDS+235 means INT with IDS and 235-mm camera)]; column 4, grating (the number refers to line mm^{-1}); column 5, wavelength coverage; column 6, 2-pixel spectral resolution.

The spectra were all bias-subtracted in the standard fashion before being optimally extracted (Horne 1986; Marsh 1989) from the data frames. Wavelength calibration was by reference to comparison CuAr or CuNe arc lamp exposures. The response function of the atmosphere+telescope+instrument was determined by dividing the extracted standard spectrum (usually that of Feige 34) by the standard's true spectrum. The extracted supernova spectrum was then divided by the response function to provide a relatively fluxed spectrum. Finally, the absolute flux zero-point was set for each supernova spectrum by integrating the product of its relatively fluxed spectrum and the broad-band photometry filter responses and then forcing a match to the photometry taken on the same night. (If no photometry was available on a particular night, then photometry was either interpolated or taken from the literature.) There was typically a difference of 5–15 per cent between the photometry and the flux-calibrated spectra on good nights before zero-point correction. The spectra are displayed in Fig. 4. The shapes of the continua of the spectra on days 11 and 12 are unreliable, presumably due to problems in the instrumental configurations on those nights. The step seen at roughly 6250 Å on day 15 is due to a bad join between the red and blue spectra. Finally, a large step can be seen in the spectrum of day 88 at about 7000 Å. This was just added in to fill a gap in the data.

Occasionally, data of higher spectral resolution (0.8 or 1.6 Å) and limited wavelength coverage were obtained. The observational and data reduction procedures were similar to those described for the low-resolution spectra. Details are given in Table 4.

6 DISCUSSION

6.1 Bolometric light curve

We have derived the bolometric light curve using our photometry plus near-IR photometry obtained from the literature. (We use the term 'bolometric' for convenience, and stress that only optical and infrared observations were used to constrain our fits.) To obtain the bolometric light curve, it is first necessary to estimate the total extinction along the line of sight to the supernova. To get a direct estimate of the extinction we assumed that the continua of the earliest spectra were essentially blackbody, and we fitted blackbody curves with flux, temperature and extinction as free parameters. The extinction was included by multiplying the blackbody function by $10^{0.4A_V C(\lambda)}$, where $C(\lambda)$ is calculated from the empirical selective extinction functions contained in Cardelli, Clayton & Mathis (1989), and R_V (the ratio of total-to-selective absorption) is assumed to be 3.1. The model function was fitted to each observed spectrum. The region

Table 3. Low-resolution spectroscopic observations of SN1993J.

Date	ΔD	Telescope/Instrument	Grating	$\lambda\lambda$(Å)	$\Delta\lambda$(Å)
Mar 29.88	2.38	INT/IDS+235	300V	4870–8700	6.2
Mar 30.88	3.38	INT/IDS+235	300V	3020–10380	6.2
Apr 01.05	4.55	INT/IDS+500	150V	3120–8230	6.0
Apr 02.02	5.52	INT/IDS+500	150V	3150–8160	11.8
Apr 03.03	6.53	INT/IDS+235	150V	2980–10290	12.2
Apr 03.98	7.48	INT/IDS+235	150V	2970–10400	12.4
Apr 05.02	8.52	INT/IDS+235	150V	2990–10420	12.4
Apr 06.02	9.52	INT/IDS+235	150V	2980–10410	12.4
Apr 07.10	10.60	INT/IDS+235	150V	3100–10410	12.4
Apr 07.84	11.34	WHT/ISIS	158B,158R	3700–8970	5.4
Apr 08.85	12.35	WHT/ISIS	158B,158R	3100–8960	5.4
Apr 09.93	13.43	WHT/ISIS	158B,158R	3370–8700	5.4
Apr 10.98	14.48	WHT/ISIS	158B,158R	3380–8780	5.4
Apr 11.95	15.45	WHT/ISIS	158B,158R	3380–8810	5.4
Apr 12.98	16.48	WHT/ISIS	158B,158R	3390–8530	5.4
Apr 16.06	19.56	WHT/ISIS+FOS2	158B	3170–9850	5.8
Apr 17.05	20.55	WHT/ISIS+FOS2	158B	3320–9850	5.8
Apr 19.06	22.56	WHT/ISIS	158B,158R	3340–8700	5.4
Apr 22.87	26.37	WHT/ISIS	158B,158R	3120–8580	5.4
Apr 28.03	31.53	INT/IDS+235	300V	3020–9880	6.2
Apr 29.86	33.36	INT/IDS+235	300V	3030–9870	6.2
May 01.87	35.37	INT/IDS+500	150V	3030–9590	5.8
May 06.88	40.38	INT/IDS+500	150V	3000–9550	5.8
May 11.89	45.39	INT/IDS+500	150V	3280–9680	5.8
May 14.86	48.36	INT/FOS1		3890–10000	10.6
May 16.86	50.36	INT/FOS1		3890–10000	10.6
May 20.86	54.36	INT/FOS1		3380–10450	10.8
May 24.90	58.40	INT/IDS+235	300V	4540–9789	6.2
May 27.86	61.36	INT/IDS+235	300V	5940–9780	6.2
May 31.90	65.40	INT/IDS+500	150V	4030–9770	5.8
Jun 08.08	72.58	WHT/ISIS	158B,158R	3290–8730	5.4
Jun 14.89	79.39	WHT/ISIS red	316R	7720–9460	3.2
Jun 15.89	80.39	INT/IDS+235	300V	3260–9780	6.2
Jun 23.90	88.40	INT/IDS+235	300V	3170–10920	6.2
Jun 24.90	89.40	WHT/ISIS	158B,158R	3370–11270	5.8
Jun 28.89	93.39	INT/IDS+235	300V	3540–7380	6.2
Jul 03.92	98.42	INT/IDS+500	300V	3610–7240	3.0
Jul 04.92	99.42	WHT/ISIS	300B,158R	3110–11130	2.9
Jul 09.90	104.40	INT/IDS+500	150V	3380–9850	5.8
Jul 12.88	107.38	INT/FOS1		3380–10660	10.8
Jul 20.90	115.40	WHT/ISIS blue	300B	4280–5720	3.0
Jul 20.90	115.40	WHT/ISIS red	316R	8000–9660	2.8

between $\lambda\lambda$4000 and 5070 was not considered in the fit in order to avoid very rapidly growing P Cygni features.

Fits were attempted for the earliest five spectra. Owing to the lack of blue coverage on day 2.4 and the very high temperature still present on day 3.4 ($T > 22\,000$ K), we were unable to achieve unique fits for these epochs. However, for the next three days good fits were achieved. The values for A_V, temperature and bolometric luminosity are presented in Table 5. It can be seen that, to within the error, the same value of A_V was obtained for all three days, in spite of a rapidly decreasing temperature. This tends to support our reddened blackbody model. The mean value of $A_V = 0.58 \pm 0.05$, and we adopt this in our determination of the bolometric light curve. This value is consistent with estimates made by Wheeler et al. (1993) using a similar method, by Schmidt et al. (1993) from the colour of the early light curve, and by Sonneborn (1993) from the 2200-Å feature.

For each date on which we acquired photometry (Table 2), a complete set of *UBVRIJHK* magnitudes has been assembled. This was done by interpolating to these dates using photometric data in the literature, as well as our own data. The infrared data were taken from measurements by Lawrence et al. (1993). These magnitudes were then de-reddened using the value of $A_V = 0.58$ obtained above, and converted to fluxes using calibrations given by Bessell (1979) for U to I_C and by Wilson et al. (1972) for J, H and K. We used two methods of estimating the bolometric flux. The first involves least-squares fitting of a Planck function to the fluxes, which has the advantage of providing estimates of several useful physical quantities. The photospheric temperature is estimated from the blackbody fits. The total flux

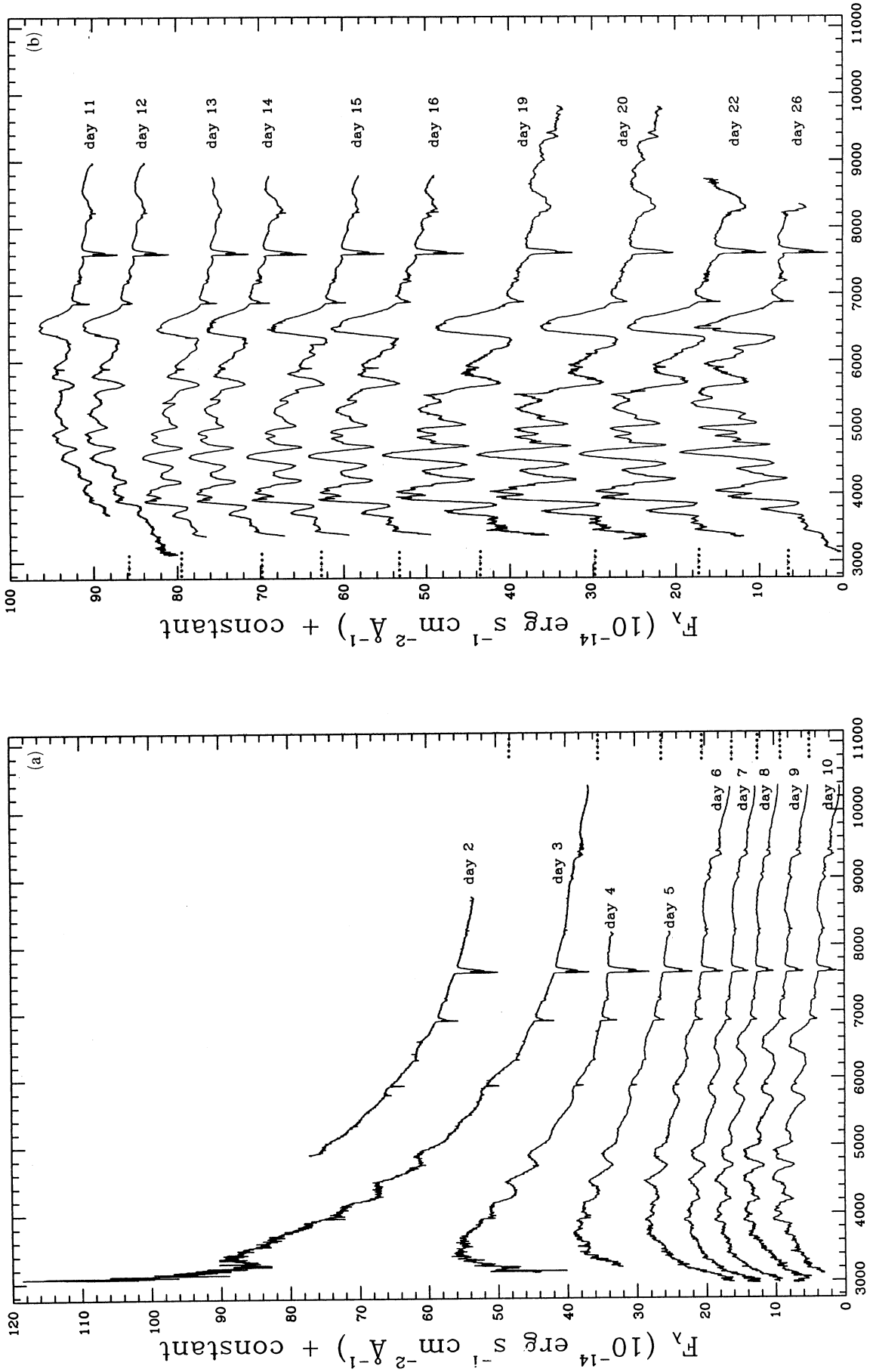

Figure 4. Evolution of the optical spectra of SN1993J. The day numbers are with respect to the adopted shock breakout time of 1993 March 27.5 (t_0). All but the final spectrum in each panel have been displaced vertically for clarity. The zero-point of each spectrum is shown by the horizontal dotted line at the right-hand edge (a) or left-hand edge (b–d). (Spectra on days 11 and 12 have badly distorted continua.)

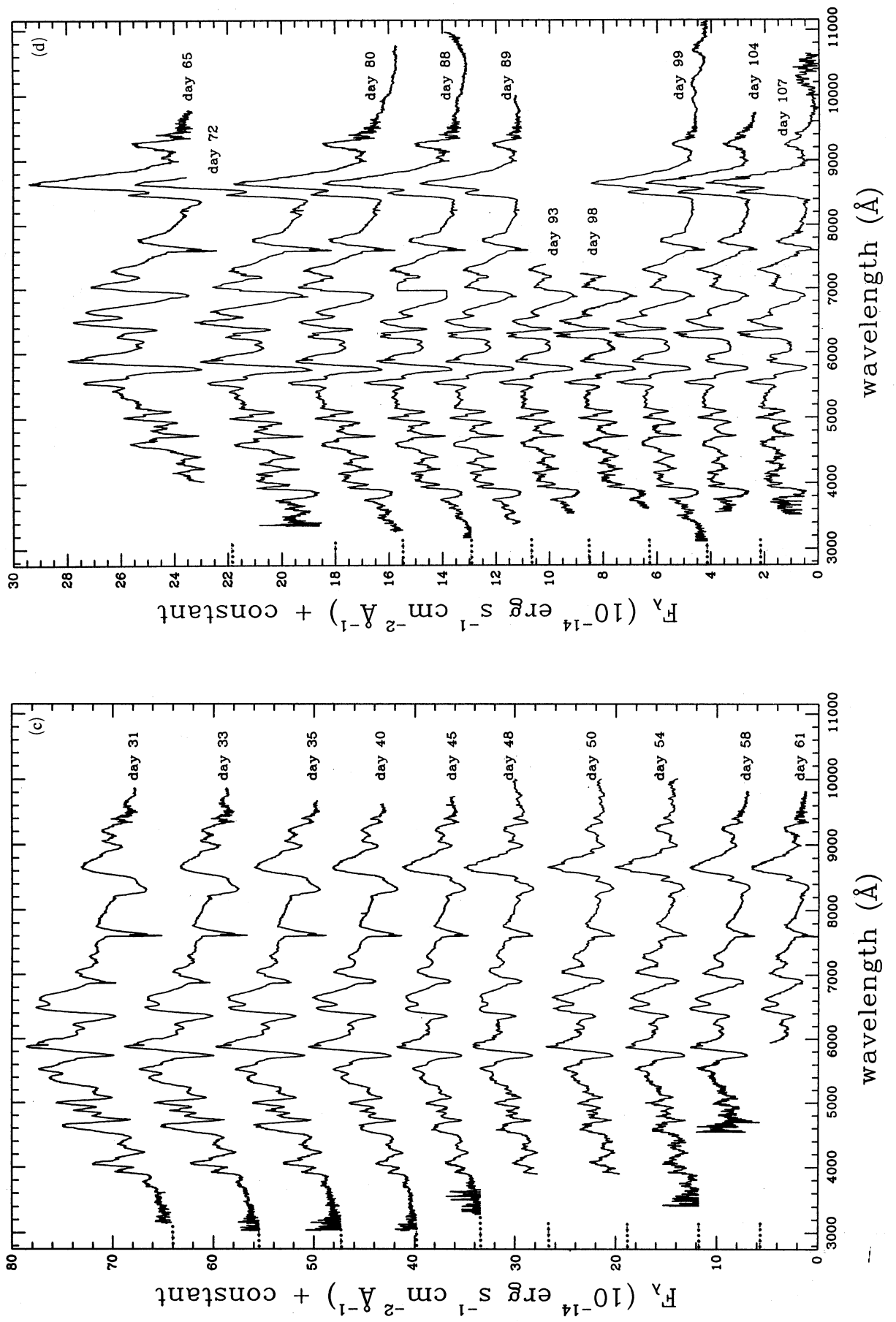

Figure 4 – *continued*

Table 4. High-resolution spectroscopic observations of SN1993J.

Date (UT)	ΔD	Telescope/Instrument	Grating	$\lambda\lambda$(Å)	$\Delta\lambda$(Å)
Apr 04.87	8.37	WHT/ISIS blue	1200R	6380–6790	0.8
May 21.86	55.36	INT/IDS+235	1200Y	6240–7110	1.6
May 21.88	55.38	INT/IDS+235	1200Y	4040–4400	1.6
May 28.88	62.38	INT/IDS+500	1200Y	6350–6800	0.8
Jun 01.89	66.39	INT/IDS+500	1200Y	6390–6840	0.8
Jun 14.89	79.39	WHT/ISIS blue	1200R	6430–6840	0.8
Jun 24.88	89.38	WHT/ISIS blue	1200B	4570–4980	0.8
Jun 24.88	89.38	WHT/ISIS red	1200R	6230–6690	0.8
Jul 05.03	99.53	WHT/ISIS blue	1200B	4450–4920	0.8
Jul 05.03	99.53	WHT/ISIS red	1200R	6380–6840	0.8

Table 5. Results of blackbody fits to early spectra.

Date (UT)	ΔD	T (K)	A_V (mag)	L (10^{40} ergs s^{-1})
Apr 01.05	4.55	13331 ± 411	0.61 ± 0.05	545.6
Apr 02.02	5.52	10666 ± 389	0.57 ± 0.08	283.1
Apr 03.03	6.53	9412 ± 429	0.54 ± 0.11	169.7

implied (from σT^4) then gives an estimate of the angular radius. The angular radius combined with an estimate of the distance gives the photospheric radius and the absolute luminosity. The second method fits spline curves as described in Hill (1982). The bolometric flux is obtained by integrating under the curve. The limits are set by assuming zero flux at zero frequency and zero flux at the frequency intercept of a line drawn through the extrapolation of the *U* and *B* points. Examples of Planck blackbody and spline fits are shown for representative days in Fig. 5. For the first few days after the explosion, the luminosities given by the blackbody-derived curve are probably more reliable. After this, the spline curve is a better representation of the true bolometric flux. During this later period, the blackbody fit becomes poorer as line emission becomes increasingly prominent, and it also overestimates the UV contribution. The bolometric fluxes were converted to luminosities by adopting a distance to M81 of 3.49 Mpc, which is the mean value quoted by Freedman et al. (1993) for a variety of methods, including their recent *HST* Cepheid result. We assume the flux equivalent of $m_{bol} = 0.0$ to be 2.795×10^{-8} W m^{-2}.

The derived bolometric luminosities, magnitudes, photospheric temperatures and radii are listed in Table 6 (the luminosities are estimated from the blackbody fits) and plotted in Fig. 6. The temperatures for days 4.4, 5.4 and 6.4 can be compared with those given in Table 5. The latter tend to be 5–10 per cent higher, although we feel that this is acceptable given the uncertainties in the two procedures used. Also shown in Table 5 are the bolometric luminosities derived from the blackbody fits to the spectra. It can be seen that similar values are obtained from blackbody fits to spectra and to photometry. The shapes of the bolometric light curves derived by the blackbody and spline fittings are very similar.

The bolometric light curve can be divided into four phases.

(i) *The first 9 d.* The luminosity had risen sharply and was already declining rapidly by the time of our first point on day 3.4, reaching a minimum on about day 9. Between days 3.4 and 9.5 the luminosity declined by nearly a factor of 10, and the temperature fell from 17 000 K to 8100 K. For the first

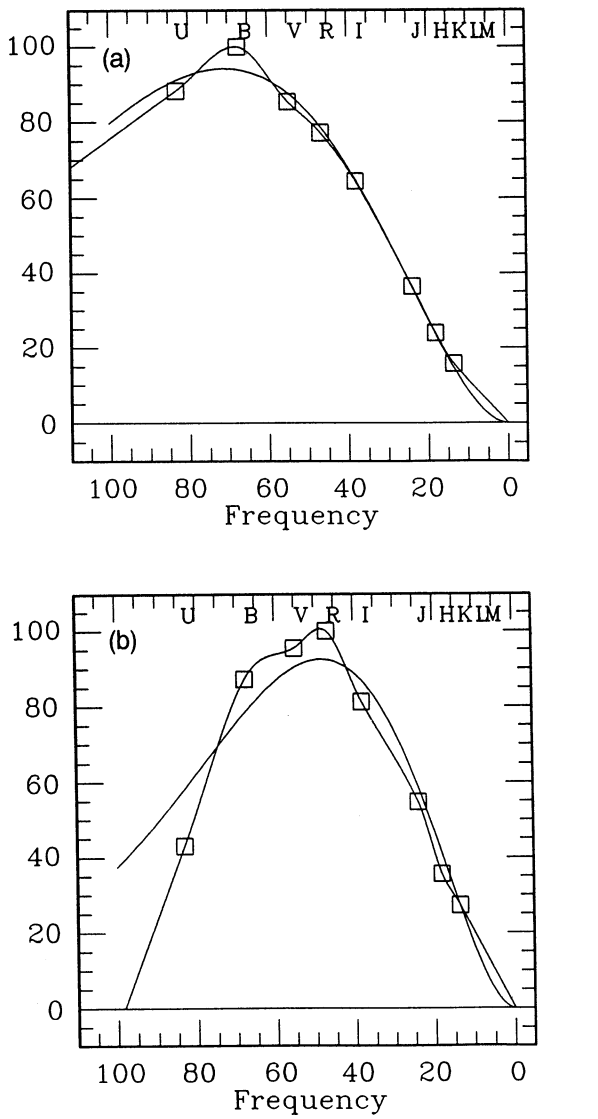

Figure 5. Sample blackbody and spline fits to the photometry for days (a) 4.48 and (b) 17.59. The ordinate represents F_ν in arbitrary units.

five days the photosphere expanded at about 13 000 km s^{-1}. Its expansion then appears to have halted for the following 4 d. This initial 9-d phase has been associated with the release from the supernova of the shock-deposited energy. The short time-scale has led to the conclusion that the H/He envelope had a mass of less than 0.5 $M_\odot$ (Podsiadlowski et al. 1993; Shigeyama et al. 1993; Wheeler et al. 1993; Woosley et al. 1993). (For a different interpretation, see Höflich, Langer & Duschinger 1993.)

(ii) *Days 9 to 21.* During this period the luminosity rose to a second maximum. The temperature remained approximately constant at 8000 K, and the photosphere began to expand again, but now at only 4000 km s^{-1}. This second rise has been associated with the escape of thermal energy previously generated by the decay of ^{56}Ni created in the explosion and its decay product ^{56}Co. The intensity of the second peak is reproduced with a ^{56}Ni mass of about 0.1 $M_\odot$ (Podsiadlowski et al. 1993; Shigeyama et al. 1993; Wheeler et al.

Table 6. Photospheric temperature and radius evolution, based on the blackbody fits to the photometry.

Date (UT)	ΔD	T (K)	R (10^{-10} radians)	R (10^{14} cm)	L (10^{40} ergs s^{-1})	M_{bol} (BB)	M_{bol} (spline)
Mar 30.89	3.39	16560	0.413	4.44	1054.6	8.96	–
Mar 31.06	3.56	16820	0.392	4.22	1014.9	9.00	–
Mar 31.98	4.48	12060	0.506	5.44	446.4	9.90	9.96
Apr 01.90	5.40	9938	0.577	6.20	267.5	10.45	10.65
Apr 02.08	5.58	9888	0.567	6.09	252.7	10.51	10.61
Apr 02.99	6.49	9174	0.566	6.08	186.7	10.84	11.02
Apr 03.16	6.66	8750	0.609	6.54	178.8	10.89	11.09
Apr 03.90	7.40	8578	0.581	6.24	150.5	11.08	11.24
Apr 04.09	7.59	8589	0.569	6.11	144.8	11.12	11.28
Apr 04.95	8.45	8487	0.563	6.05	135.2	11.19	11.32
Apr 05.08	8.58	8407	0.569	6.12	133.1	11.21	11.34
Apr 05.91	9.41	8145	0.609	6.55	134.4	11.20	11.35
Apr 05.97	9.47	8156	0.606	6.52	134.0	11.20	11.37
Apr 06.10	9.60	8141	0.611	6.56	134.9	11.20	11.36
Apr 06.99	10.49	7977	0.648	6.97	140.0	11.16	11.33
Apr 08.02	11.52	7945	0.691	7.43	156.9	11.03	11.24
Apr 08.10	11.60	8017	0.681	7.32	157.8	11.03	11.24
Apr 08.98	12.48	7913	0.739	7.94	176.4	10.90	11.12
Apr 10.07	13.57	8087	0.742	7.97	193.9	10.80	11.04
Apr 10.16	13.66	8144	0.736	7.91	196.1	10.79	11.04
Apr 10.89	14.39	7820	0.836	8.98	215.1	10.69	10.93
Apr 10.93	14.43	7751	0.852	9.15	215.6	10.69	10.91
Apr 11.01	14.51	7912	0.812	8.73	212.9	10.70	10.95
Apr 11.06	14.56	7840	0.822	8.84	210.4	10.71	10.95
Apr 11.93	15.43	8158	0.800	8.60	233.6	10.60	10.83
Apr 12.87	16.37	8174	0.828	8.90	252.1	10.52	10.78
Apr 13.00	16.50	8011	0.861	9.25	251.2	10.52	10.76
Apr 13.88	17.38	7829	0.924	9.93	263.9	10.47	10.71
Apr 14.04	17.54	8192	0.855	9.19	271.3	10.44	10.69
Apr 14.88	18.38	7945	0.926	9.95	281.1	10.40	10.65
Apr 14.98	18.48	8203	0.877	9.43	287.0	10.38	10.63
Apr 15.88	19.38	7803	0.975	10.48	290.0	10.36	10.62
Apr 16.05	19.55	8160	0.899	9.67	295.3	10.35	10.60
Apr 16.89	20.39	7852	0.977	10.50	298.5	10.33	10.58
Apr 17.00	20.50	8190	0.907	9.75	304.6	10.31	10.56
Apr 17.93	21.43	8016	0.936	10.06	297.8	10.34	10.57
Apr 21.96	25.46	6674	1.238	13.31	250.3	10.52	10.74
Apr 23.91	27.41	6333	1.255	13.49	208.6	10.72	10.96
Apr 24.89	28.39	6093	1.292	13.89	189.5	10.83	11.04
Apr 25.91	29.41	5835	1.391	14.95	184.6	10.85	11.09
Apr 27.91	31.41	5638	1.396	15.00	162.1	11.00	11.25
Apr 28.87	32.37	5548	1.390	14.94	150.7	11.08	11.34
Apr 29.90	33.40	5425	1.442	15.50	148.4	11.09	11.35
Apr 30.88	34.38	5411	1.409	15.15	140.2	11.15	11.42
May 05.89	39.39	6009	0.990	10.64	105.1	11.47	11.62
May 14.90	48.40	6006	0.877	9.43	82.5	11.73	11.88
May 15.90	49.40	5988	0.867	9.32	79.6	11.77	11.91
May 16.88	50.38	5984	0.856	9.20	77.3	11.80	11.94
May 18.99	52.49	6005	0.832	8.94	74.1	11.85	11.99
May 22.88	56.38	6102	0.778	8.36	69.1	11.92	12.07
May 24.91	58.41	6116	0.759	8.15	66.3	11.97	12.12
May 25.88	59.38	6143	0.744	8.00	64.9	11.99	12.14
Jun 19.90	84.40	6653	0.508	5.46	41.5	12.47	12.65
Jun 20.94	85.44	6667	0.503	5.40	41.1	12.49	12.66
Jun 21.92	86.42	6712	0.493	5.29	40.5	12.50	12.68
Jun 23.92	88.42	6749	0.480	5.15	39.3	12.53	12.72
Jul 15.94	110.44	7235	0.345	3.71	26.9	12.95	13.16
Jul 30.93	125.43	7546	0.279	2.99	20.7	13.23	13.46

1993; Woosley et al. 1993). Shigeyama et al. (1993) find that the epoch of the second peak indicates a zero-age main-sequence mass of about $15\,M_{\odot}$ for the progenitor, of which $10\,M_{\odot}$ would have been the hydrogen envelope. The low mass of the hydrogen envelope when the star exploded implies an enormous mass loss before the supernova occurred. The most popular view is that this material was lost through interaction with a close companion star (Podsiadlowski et al. 1993; Woosley et al. 1993).

The constancy of the temperature during this phase probably indicates that the photosphere was then defined by the recombination wave of the H/He envelope. The speed at which the recombination front moved into the material would have been slowed by the energy released from the decaying ^{56}Ni and ^{56}Co, producing the observed rate of expansion of the photosphere.

(iii) *Days 21 to 50.* At the start of this phase the luminosity began to decline and the temperature dropped sharply. This

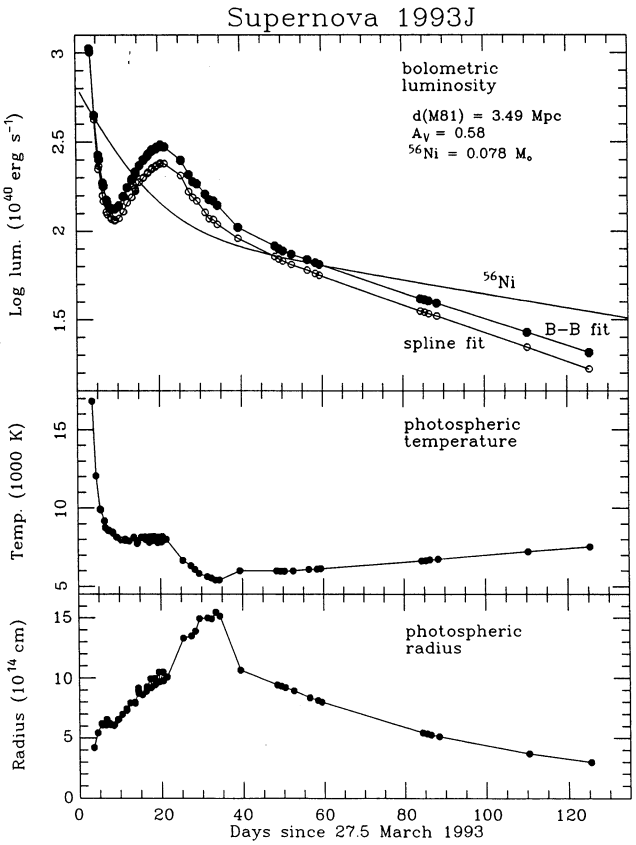

Figure 6. Upper panel: the bolometric light curve for blackbody fits (solid symbols) and for spline fits (open symbols). Also shown in this panel is the luminosity decay curve for 0.078 $M_\odot$ of ^{56}Ni. The middle and lower panels show the evolution of the photospheric temperature and radius.

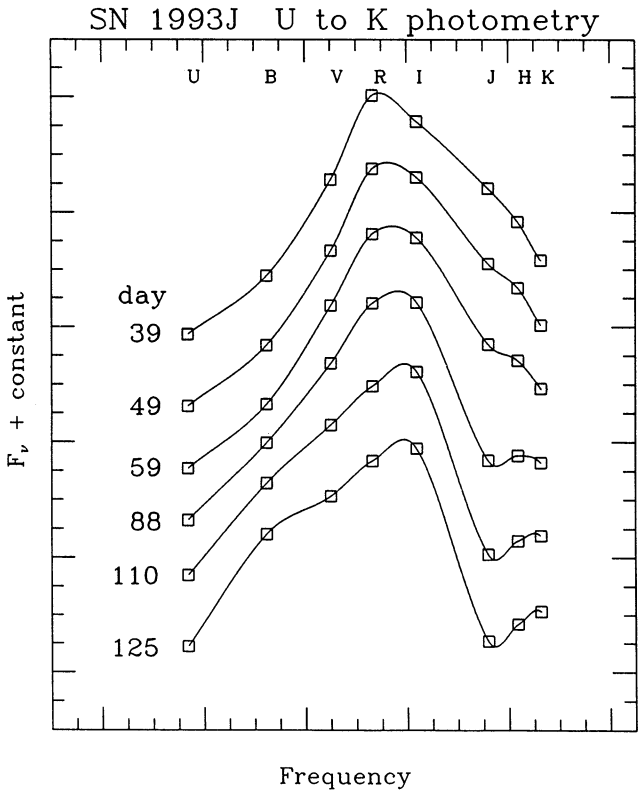

Figure 7. Spline fits to photometry for six representative days. The excess in the infrared is clearly evident in the latest three. The IR photometry was obtained by interpolating the measurements of Lawrence et al. (1993) to the epochs of our optical observations.

event may have been due to the recombination front reaching the boundary between the H/He envelope and the purer He mantle. Since the mantle would have had a higher recombination temperature, it would already have recombined by day 21. Consequently, the photosphere receded rapidly inward and the ejecta became increasingly nebular. A blackbody spectrum became decreasingly representative of the actual spectrum, and so the derived photospheric temperature and radius probably have less and less physical meaning beyond day 21.

(iv) *After day 50.* After about day 50 the luminosity (spline fit) declined exponentially with an e-folding time of 54 d. This is considerably faster than the 111.3-d e-folding time for the decay luminosity of ^{56}Co (Fig. 6), and indicates that by day 50 a significant proportion of the decay gamma-rays were escaping. Unlike SN1987A, SN1993J never went through a phase when the bolometric luminosity matched the ^{56}Co decay rate. Presumably this was due to the much lower mass of SN1993J. Consequently, it is difficult to obtain directly the initial ^{56}Ni mass from the light curve. Models that take into account the changing opacity to gamma-rays indicate a ^{56}Ni mass very similar to the 0.078 $M_\odot$ seen in SN1987A (Podsiadlowski et al. 1993; Shigeyama et al. 1993; Wheeler et al. 1993; Woosley et al. 1993).

From our optical photometry and from interpolated IR photometry based on the measurements of Lawrence et al. (1993), we deduce that near the start of this period an infrared excess appeared (Fig. 7), peaking beyond the *K* window. The implications of this excess for the bolometric light curve depend on its origin. If it is due to line emission from or dust condensation in the ejecta, then the lack of spectral coverage beyond the *K* window means that the bolometric luminosity is underestimated. However, if the excess is due to an IR echo from dust in the circumstellar medium of the progenitor, lying at a large distance from the supernova, then the excess should not be added to the late-time luminosity, but rather should be added to the luminosity near maximum. (This assumes a uniform spherical shell geometry for the medium.) The contribution of the IR echo to the light curve near peak would be relatively small.

It is difficult to see how line emission could account for the IR excess, as such emission would have to affect the *H* and *K* windows much more strongly than in the optical region. One possibility is CO emission. This has its first overtone in *K* and its second in *H*. However, the similarity of the fluxes at *H* and *K* argues against this hypothesis. For SN1987A, the second-overtone intensity was expected to be only 1.4 per cent that of the first overtone, and indeed no second-overtone emission was identified, even at the peak of the first-overtone emission (Spyromilio et al. 1988).

Dust condensation in the ejecta also seems unlikely. If we extrapolate the optical continuum into the near-IR and sub-

tract it, the residual IR colours indicate a temperature of about 2000 K. While dust condensation was observed in the ejecta of SN1987A, this was at a much lower temperature (800 K) and a much later epoch (1 yr). A more promising scenario is that the excess is due to an IR echo. The huge mass loss from the progenitor star suggests that there could indeed be a large mass of dust lying up to a light-year from the supernova (Woosley et al. 1993). The appearance of such an early excess has been observed before, in SN1982E (Graham et al. 1983). This was successfully interpreted (Graham et al. 1983; Graham & Meikle 1986) as being due to reradiation by a 10^{-3}-$M_{\odot}$ spherical cloud of dust grains of inner radius 0.14 light-year. In the case of SN1982E, the temperature on day 101 was 1320 K. We conclude that an IR echo could well be responsible for the IR excess, which should therefore be subtracted from the late-time bolometric light curve. Of course, the large fraction of gamma-rays that are escaping at late times means that such a light curve still grossly underestimates the true total luminosity of the ejecta.

6.2 The spectra

As has been pointed out by several groups of authors (Filippenko et al. 1993a; Schmidt et al. 1993; Swartz et al. 1993), the spectrum evolved from being that of a Type II event, characterized by prominent Balmer lines, to a spectrum which was much more akin to that of a Type Ib. In Fig. 8 likely line identifications are indicated for the day 80 (1993 June 15) spectrum. The vertical markers are placed at the rest wavelengths in the frame of M81, i.e. shifted by -135 km s^{-1} (Vladilo et al. 1993). By this time the spectrum was dominated by lines of helium, oxygen, sodium, magnesium and calcium, characteristic of a Type Ib supernova. Many of the lines exhibited blueshifts. In particular, the [O I] lines exhibited a shift of about -2000 km s^{-1}. This shift was present as early as day 50, and was still present on day 140. While some of the shifts may be due to blending with the absorption components of neighbouring lines, it is unlikely that the shift in the [O I] lines can be explained in this way. This blueshift has also been reported by Wang et al. (1993). The early appearance and unchanging nature of the blueshift argue against dust condensation being responsible. A more plausible explanation is asymmetry in the distribution of the line-emitting region. The redshift in the Ca II triplet is probably due to the blended absorption components of the multiplet. As the feature became optically thin, the redshift gradually disappeared, and had vanished by day 140.

7 SUMMARY

We have presented spectroscopic, photometric and astrometric results from a large body of observations of SN1993J

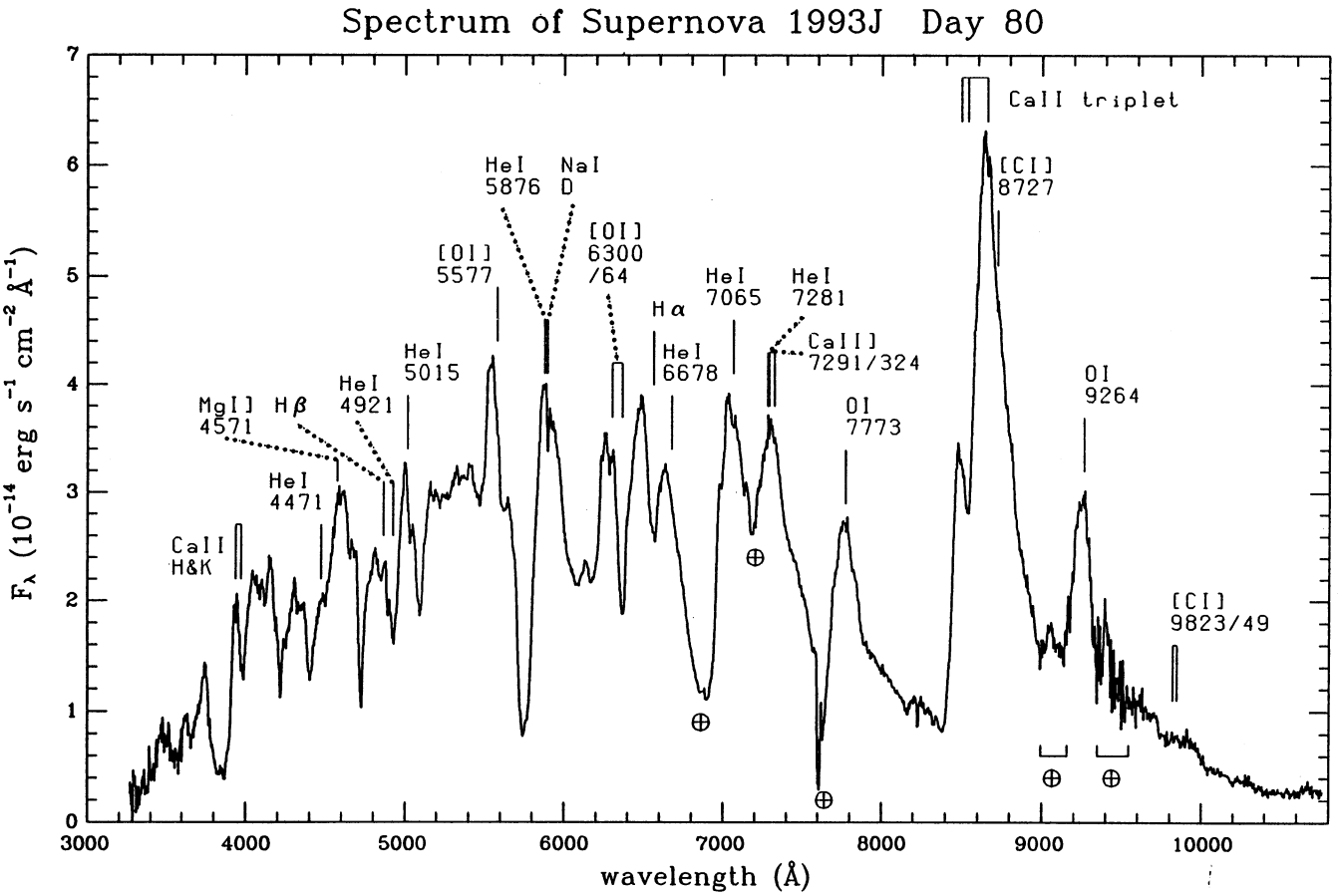

Figure 8. The low-resolution spectrum for day 80. Vertical markers are placed at the rest wavelengths in the frame of M81 (shifted by -135 km s^{-1}) indicating likely line identifications.

obtained from La Palma. The astrometric results will become very important in later epochs as the supernova fades and becomes difficult to locate even with a large telescope. A value of $A_V = 0.58$ is derived from the early spectroscopic data, and is combined with the photometry to produce a *U*-to-*K* bolometric light curve. This shows double maxima followed by an exponential decay with an e-folding time of about 54 d, suggesting that after day 50 much of the flux is lost in γ- and X-rays. An infrared excess, which appeared after day 50, may be indicative of an IR echo. Blue-shifted oxygen lines in the spectra argue for asymmetry in the distribution of the line-emitting region.

ACKNOWLEDGMENTS

A project of this size would be impossible were it not for the co-operation of a very large number of people. In particular, we thank all the observers, especially those not listed amongst the authors, who graciously gave up significant amounts of their hard-won observing time in order that the monitoring of SN1993J could proceed. These are M. Breare, F. Carrera, E. Conlon, H. Ferguson, P. García-Lario, I. Gonzales-Serrano, R. de Grijs, I. Hook, M. Irwin, E. Martinez-Gonzalez, the MARTINI group, M. Pettini, T. Ray, A. Sansom, L. Storrie-Lombardi and R. Terlevich. We also thank the following: Professor G. de Vaucouleurs for suggestions on improving the photometric results; Dr P. Podsiadlowski for very helpful discussions on the interpretation of the bolometric light curve; Dr R. C. Thomson for much useful advice on data reduction; Ms J. Compagnoni and Mr R. A. Knight for their help in transferring some of the data from La Palma to Cambridge; Mr A. N. Johnson for his help in preparing some of the diagrams; Mr E. Telles and the GEFE group for providing us with the progenitor CCD frames of SN1993J; Dr J. D. H. Pilkington for scanning plates of M81 on the PDS; Dr T. Kato for his work in maintaining a photometric data compilation of SN1993J; and finally the long-suffering system managers in Cambridge, Messrs P. Herridge, G. Lewis and S. Percival, for putting up with a seemingly endless stream of requests. The ING telescopes and the CAMC are located on the island of La Palma in the Spanish Observatorio del Roque de los Muchachos of the Instituto de Astrofísica de Canarias. The ING telescopes are operated by the Royal Greenwich Observatory (RGO) and the CAMC is operated jointly by Copenhagen University Observatory, RGO, and the Instituto y Observatorio de la Armada, Spain.

REFERENCES

Allington-Smith J. R. et al., 1989, MNRAS, 238, 603
Argyle R. W., Mayer C. J., Pike C. D., Jorden P. R., 1988, A User Guide to the JKT CCD Camera. RGO Publication
Benn C., Nicholson D., 1988, Filter and CCD chip spectral-response curves for La Palma. RGO Publication
Bessell M. S., 1979, PASP, 91, 589
Blakeslee J., Tonry J., 1993, IAU Circ. 5758
Cardelli J., Clayton G., Mathis J., 1989, ApJ, 345, 245
Clegg R. E. S., Carter D., Charles P. A., Dick J. S. B., Jenkins C. R., King D. L., Laing R. A., 1992, ISIS Astronomers' Guide. RGO Publication
Filippenko A. V., Matheson T., Ho L. C., 1993a, ApJ, 415, L103
Filippenko A. V., Treffers R. R., Paik Y., Davis M., Schlegel D., 1993b, IAU Circ. 5731
Freedman W. L. et al., 1993, BAAS, 25, 914
García F., 1993, IAU Circ. 5731
Garnavich P., Ann H. B., 1993, IAU Circ. 5731 (Corrigendum: IAU Circ. 5733)
Graham J. R., Meikle W. P. S., 1986, MNRAS, 221, 789
Graham J. R. et al., 1983, Nat, 304, 709
Helmer L., Fabricius C., Morrison L. V., 1991, Exp. Astron., 2, 85
Hill G., 1982, Publ. Dom. Astrophys. Obs., 16, 67
Höflich P., Langer N., Duschinger M., 1993, A&A, 275, L29
Horne K., 1986, PASP, 98, 609
Humphreys R. M., Aldering G. S., Bryja C. O., Thurmes P. M., 1993, IAU Circ. 5739
Kato T., 1993, Notes in Nova News Network
Landolt A., 1983, AJ, 88, 439
Landolt A., 1992, AJ, 104, 340
Lawrence G. F., Paulson A., Mason C., Butenhoff C., Gehrz R. D., 1993, IAU Circ. 5844
Marsh T. R., 1989, PASP, 101, 1032
Marcaide J. M. et al., 1993, IAU Circ. 5820
Massey P., Strobel K., Barnes J. V., Anderson W., 1988, ApJ, 328, 35
Merlin J.-C., 1993, IAU Circ. 5740
Morrison L. V. et al., 1990, A&A, 240, 173
Morrison L. V., Argyle R. W., Helmer L., 1993, IAU Circ. 5767
Neely A. W., 1993a, IAU Circ. 5740
Neely A. W., 1993b, IAU Circ. 5832
Podsiadlowski Ph., Hsu J. J. L., Joss P. C., Ross R. R., 1993, Nat, 364, 509
Prugniel P., 1993, IAU Circ. 5742
Richmond M., 1993a, Notes in Nova News Network
Richmond M., 1993b, IAU Circ. 5739
Rodriguez D., 1993, IAU Circ. 5731
Schmidt B. P. et al., 1993, Nat, 364, 600
Shigeyama T., Suzuki T., Kumagai S., Nomoto K., Saio H., Yamaoka H., 1993, ApJ, in press
Solberg R., 1993, Notes in Nova News Network
Sonneborn G., 1993, in Clegg R. E. S., Meikle W. P. S., Stevens I. R., eds, Proc. 34th Herstmonceux Conf., Circumstellar Media in the Late Stages of Stellar Evolution. Cambridge Univ. Press, Cambridge, in press
Spyromilio J., Meikle W. P. S., Learner R. C. M., Allen D. A., 1988, Nat, 334, 327
Swartz D. A., Clocchiatti A., Benjamin R., Lester D. F., Wheeler J. C., 1993, Nat, 365, 232
Terlevich E., Terlevich R. J., Charles P. A., 1989, Spectroscopy with the CCD on the INT. RGO Publication
Ulfheden P., Hamberg I., 1993, Notes in Nova News Network
Vladilo G., Centurión M., de Boer K. S., King D. L., Lipman K., Unger S. W., Walton N. A., 1993, A&A, 280, L11
Wang L., Hu J. Y., Li A. G., Li H. B., 1993, IAU Circ. 5847
Wheeler J. C. et al., 1993, ApJ, 417, L71
Wilson W. J., Schwartz P. R., Neugebauer G., Harvey P. M., Becklin E. E., 1972, ApJ, 177, 523
Woosley S. E., Eastman R. G., Weaver T. A., Pinto P. A., 1993, ApJ, preprint